applied optics

On the performance of adaptive hybrid *M*QAM–MPPM scheme over Nakagami and log-normal dynamic visible light communication channels

Abd El-Rahman A. El-Fikky,[1] Abdallah S. Ghazy,[2] Haitham S. Khallaf,[3,6] Ehab Mahmoud Mohamed,[4,7] Hossam M. H. Shalaby,[5,8] and Moustafa H. Aly[1,*]

[1]College of Engineering and Technology, Arab Academy for Science, Technology and Maritime Transport, Alexandria 1029, Egypt
[2]Department of Electronics and Communications Engineering, McMaster University, Ontario, Canada
[3]Nuclear Research Center, Egyptian Atomic Energy Authority (EAEA), Inshas 13759, Egypt
[4]College of Engineering, Prince Sattam Bin Abdulaziz University, Wadi Aldwaser 11991, Saudi Arabia
[5]Electrical Engineering Department, Alexandria University, Alexandria 21544, Egypt
[6]Graduate School of Information Science and Electrical Engineering, Kyushu University, Japan
[7]Electrical Engineering Department, Faculty of Engineering, Aswan University, Aswan 81542, Egypt
[8]Department of Electronics and Communications Engineering, Egypt-Japan University of Science and Technology (E-JUST), Alexandria 21934, Egypt
*Corresponding author: mosaly@aast.edu

Received 9 October 2019; revised 11 December 2019; accepted 9 January 2020; posted 10 January 2020 (Doc. ID 379893); published 21 February 2020

In this paper, we introduce the idea of using adaptive hybrid modulation techniques to overcome channel fading effects on visible light communication (VLC) systems. A hybrid *M*-ary quadrature-amplitude modulation (*M*QAM) and multipulse pulse-position modulation (MPPM) technique is considered due to its ability to make gradual changes in spectral efficiency to cope with channel effects. First, the Zemax optics studio simulator is used to simulate dynamic VLC channels. The results of Zemax show that Nakagami and log-normal distributions give the best fitting for simulation results. The performance of *M*QAM–MPPM is analytically investigated for both Nakagami and log-normal channels, where we obtain closed-form expressions for the average bit-error rate (BER). The optimization problem of evaluating the hybrid modulation technique settings that lead to the highest spectral efficiency under a specific channel status and constraint of outage probability is formulated and solved using an exhaustive search. Our results reveal that the adaptive hybrid scheme improves system spectral efficiency compared to ordinary QAM and MPPM schemes. Our results reveal that the adaptive hybrid scheme improves system spectral efficiency compared to ordinary QAM and MPPM schemes. Specifically, at low average transmitted power, −32 dBm, the adaptive hybrid scheme shows 280% improvement in spectral efficiency compared to adaptive versions of ordinary schemes. At higher power, −20 dBm, 6.5% and 725% improvement are obtained compared to ordinary QAM and ordinary MPPM, respectively. Also, the adaptive hybrid scheme shows great improvement in average BER and outage probability compared to ordinary schemes. The hybrid scheme shows 28%, 34%, and 38% improvement, respectively, for $m = 1, 2, 3$ for Nakagami channels at BER$= 10^{-3}$. Also, the outage probability of hybrid schemes of BER$= 10^{-3}$ shows 30% and 14% better performance than ordinary *M*QAM and MPPM schemes, respectively. © 2020 Optical Society of America

https://doi.org/10.1364/AO.379893

1. INTRODUCTION

Over the last years, the demand for wireless communication has increased dramatically, and concern for spectral efficiency is growing due to the scarcity of the radio frequency (RF) spectrum [1]. Unlicensed wide frequency spectrum is becoming very prevalent in the modern architecture of mobile communications networks, car-to-car communication, and communication inside nuclear facilities, in order to exploit its unlimited features, e.g., wide-free frequency spectrum, low transmitted power, low cost, easy installation, and security of communication [2,3]. However, there are some challenges that need to be addressed in order to mitigate their effects. One of the major challenges in VLC systems is the narrow bandwidth of conventional LEDs,

which leads to a limitation of maximum achievable data rates that can be transmitted using VLC systems. Furthermore, as a wireless communication system, VLC is highly affected by fading and shadowing, which results in variation in the amplitude and phase of the received signal and causes degradation of system performance. These two challenges motivate researchers to work on increasing spectral efficiency and to obtain an accurate model for fading VLC channels.

The choice of a suitable modulation technique is one of the important factors that affects communication system performance and can be considered a solution to overcome the bandwidth limitation of LEDs in VLC systems. This point has been investigated in many papers. In Ref. [4], the performance of optical wireless communications adopting different pulse time modulation techniques has been investigated and compared to on–off keying (OOK), pulse-position modulation (PPM), differential pulse interval modulation (D-PIM), and double-header PIM (DH-PIM) techniques. The performances of differential binary phase shift (DBPSK) and differential quadrature phase shift key (DQPSK) were investigated in optical communication systems for wavelength-division multiplexing schemes by Morsy *et al.* [5].

In Ref. [6], the implementation of carrier-less amplitude and phase modulation in VLC systems was introduced and its bit-error rate (BER) and average throughput performance evaluated. The performance of a multiple-input–multiple-output orthogonal frequency-division multiplexing (MIMO-OFDM) VLC system was demonstrated experimentally in Ref. [7]. The idea of superimposing different modulation techniques, to enhance both power and spectral efficiencies simultaneously, has been shown in many recent studies [8–12].

A good description and modeling for VLC channels are major factors that can help in the design optimization and performance evaluation of VLC systems. Usually, Lambertian distribution is used to model the static/quasi-static channel, where the large-scale effect (path loss) is the dominant challenge[1].

In Ref. [13], the effect of atmospheric scattering, attenuation, turbulence, and scintillation is examined for free-space optics systems at 850 and 1550 nm. However, in the dynamic environment, due to people's mobility inside a VLC cell, the wireless links are subject to severe multipath and random shadowing (blockage) fading, as illustrated in Ref. [14]. Modeling of a static VLC channel has been investigated many times in literature [15,16]. However, a static channel does not represent the real case, because usually people are using mobile equipment or the surrounding people are in motion states.

This is why the recent modeling of dynamic VLC channels has attracted many researchers. In Ref. [14], the user mobility effect on VLC channel gain is experimentally evaluated by representing the human body as a box shape and moving these boxes manually between transmitter and receiver. The authors show that Rayleigh distribution achieves good fitting with their measurements. The dynamic channel modeling in underwater VLC channel modeling is investigated in Ref. [17]. The obtained results show that Weibul, log-normal, and Nakagami exhibit accepted goodness of fit results for single input single output (SISO) and single input multiple output (SIMO) models in good channel conditions. The authors show that exponential distribution is the best distribution for the specific scenarios that show worse channel conditions.

In Refs. [18,19], a study is carried out using different reflection coefficients for objects. One moving human body is configured that is carrying the receiver, and 961 receiver positions are assumed for a practical human model without considering any random motion algorithm. Furthermore, the study is performed using reflection coefficients for all objects that are independent of transmitter wavelength. Different configurations for device orientation are examined assuming static mobile users by Miramirkhani *et al.* [20]. Moreover, they assume the coating materials for walls are wavelength independent, and the obtained expressions for outage probability and BER are applied on the OOK modulation technique.

In Ref. [21], Eroglu *et al.* configure a mobile user moving in a trajectory path and obtain the channel impulse response (CIR) for each movement point. However, they do not obtain distributions that provide the maximum likelihood for the acquired data, and they do not apply the modulation techniques for BER measurements and outage probability calculations.

The results in Ref. [20] motivated us to use a practical setup Monte Carlo ray tracing (MCRT) simulator and add mobile users in a random motion manner and evaluate the obtained distributions, which exhibit a goodness of fit of the dynamic channel gain variations.

The main contribution of our paper is introducing the idea of optimizing the performance of VLC systems through using an adaptive hybrid *M*QAM–MPPM scheme to overcome fading effects. An accurate model for a dynamic VLC channel for mobile users is introduced based on the Zemax optics studio simulator, where accurate CADs for the human body are used, users with random motions are considered, and real coating materials are considered for both human bodies and surrounding objects.

The problem of optimizing the average spectral efficiency of the hybrid modulation technique over the VLC channel is formulated and solved to get the best hybrid scheme settings based on channel state.

Finally, expressions for both BER and outage probability of the proposed hybrid scheme are derived and used to evaluate system performance over different levels of fading and different people densities inside the considered standard room.

The rest of this paper is organized as follows. In Section 2, the proposed hybrid *M*QAM–MPPM system model is illustrated. In Section 3, the Zemax optics studio simulator is used to simulate a dynamic VLC channel, and the probability distribution functions (PDFs) of the received electrical signal-to-noise ratio (SNR) are determined. Expressions for average BER of the hybrid schemes is derived in Section 4. In Section 5, the problem of optimizing the average spectral efficiency of VLC systems using adaptive hybrid schemes is formulated. In Section 6, the performance of both hybrid and ordinary schemes is evaluated in terms of BER and outage probabilities over both Nakagami and log-normal VLC channels. Moreover, the performance of adaptive schemes is investigated in terms of spectral efficiency. Finally, the main conclusions are given in Section 7.

2. HYBRID MQAM–MPPM SYSTEM MODEL

The hybrid *M*QAM–MPPM scheme was introduced in Ref. [12], and its performance under different free-space optical

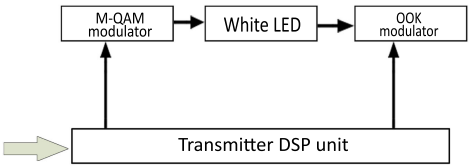

Fig. 1. Basic block diagram of a hybrid MQAM–MPPM transmitter in a VLC system.

communication channels was introduced in Ref. [22]. In this section, the main idea of the hybrid MQAM–MPPM scheme and its block diagrams for both transmitter and receiver are discussed.

In hybrid MQAM–MPPM scheme techniques, the symbol duration T is divided into N time slots, each with duration $T_s = T/N$. The optical power appears in w signal time slots only, where $w \in \{1, 2, \ldots, N\}$. Each of the optical signal slots is coded with a QAM symbol. The total number of bits per hybrid scheme symbol is $\lfloor \log_2 Nw \rfloor + w \log_2(M_q)$, where M_q is the level of QAM modulation. Figures 1 and 2 illustrate the transmitter and receiver simplified block diagrams for the hybrid scheme in a VLC system.

The output optical power of the OOK modulator is proportional to the modulating QAM signals as follows [23]:

$$P(t) = \frac{Np_t}{w} \sum_{i=0}^{N-1} [1 + MD_i(t)]\, B_i(t) \text{rect}\left(t - \frac{iT}{N}\right), \quad \textbf{(1)}$$

where p_t is the average transmitted optical power, M is the modulation index, $D_i(t)$ is the QAM symbol, $B_i(t) \in \{1, 0\}$ is the value of the MPPM slot, and the rect function is defined as

$$\text{rect}(t) = \begin{cases} 1; & 0 \le t < \frac{\text{T}}{\text{N}}, \\ 0; & \text{otherwise.} \end{cases} \quad \textbf{(2)}$$

At the receiver side, the optical signal is converted to the electrical domain through a photo-diode (PD) (Fig. 2). The instantaneous generated current $Y(t)$ from the PD is defined by Ref. [22]:

$$Y(t) = I_{ph} \sum_{i=0}^{N-1} [1 + MD_i(t)] B_i(t) \text{rect}\left(t - \frac{iT}{N}\right) + n(t), \quad \textbf{(3)}$$

where I_{ph} is the instantaneous photo-current:

$$I_{ph} = \mathcal{R} \frac{Np_t}{w} h(t), \quad \textbf{(4)}$$

where $\mathcal{R}$ is the responsivity of the PD, $h(t)$ is the CIR, and $n(t)$ is Gaussian noise with variance σ_n^2.

In our analysis, we consider perfect synchronization, where the effect of timing error is not considered. However, it is worth noting the expected effect of timing error on the proposed system performance. There are two types of timing errors: frame and time slot based. The frame-based timing error is a result of timing offsets, which are a multiple of the time slot duration. This type of the error has no effect on the performance of the MQAM–MPPM branch in the proposed scheme, since the relative phase differences between successive slots are not affected by multiple time slot offsets. The second type of timing error, time slot, is a result of time offset value Δ, where $\Delta \le 0.5$. The effect of this timing error in DPSK BER performance was discussed and investigated in Refs. [24,25]. In addition, the effects of both types of timing errors on the MPPM detection process were discussed in Refs. [26,27].

3. VISIBLE LIGHT COMMUNICATIONS CHANNEL MODEL

In this section, the Zemax optics studio [28], which is based on MCRT simulation, is used to figure out the most suitable distribution to describe the dynamic VLC channel gain. As shown in Fig. 3, we consider seven mobile users moving in random motions inside a $5 \times 5 \times 3$ m^3 room.

Each one of these mobile users is equipped with a mobile device that is able to communicate using VLC. The users are moving with speeds between 0.56 and 1.39 m/s. We assume that he/she holds a mobile phone in-hand, and the detector is located on the mobile phone with practical dimensions. The orientation of the mobile users changes between 0° and 360°, while the orientation of the mobile device is assumed to be fixed. The choice of user speed and direction is based on uniform distribution.

In our simulation, we use advanced human CADs [29], and the dimensions of the mobile users for height, width, and depth are 1.8, 0.4, and 0.2 m, respectively. The seven mobile users in the simulation are chosen according to the people density criteria > 0.16 people/m^2 to ensure the worst-case scenario conditions for fading as given in Ref. [14]. We define the positions for each human body for 1000 s according to a random motion algorithm. Each second has different positions and orientations for the seven users, and consequentially, new channel gain calculations are required for each second.

Every movement has a correlation with past movements. Furthermore, the random mobility algorithm is established

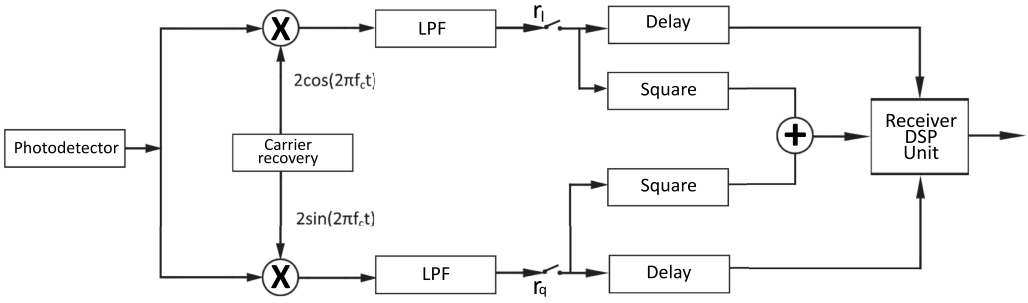

Fig. 2. Basic block diagram of a hybrid MQAM–MPPM receiver in a VLC system.

Fig. 3. Random motion for mobile users in an indoor dynamic VLC scenario for standard room dimensions.

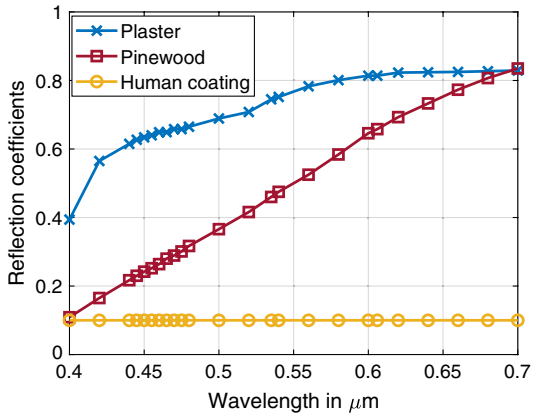

Fig. 4. Reflection coefficient at different wavelengths for material used in simulation.

using Zemax programming language (ZPL) [30], which enables us to apply 1000 iterations rather than using one specific scenario like the static configuration. In addition, different materials are considered for different objects inside the simulation area. Figure 4 shows the reflection coefficients for different materials used in our simulation.

The materials used for the ceiling, floor, and walls have variable reflection coefficients based on the transmitter wavelength. It is mandatory to use such coating configurations for the VLC channel due to the use of practical broadband white LEDs [31]. These are commercially available LEDs Cree with 120° viewing angles. We configure the mobile users' coatings to have the smallest value 0.1 that indicates maximum absorption of rays. Specifically, the coatings for heads and hands are modeled as absorbing clothes and dark skin as assumed in Ref. [18]. In addition, we consider the Lambertian model and purely diffuse material, which is considered to be the worst-case scenario in the case of specular reflections. All the simulation parameters used in the MCRT solver are illustrated in Table 1.

The CIR used in the MCRT solver is defined by Ref. [16]:

$$h(t) = \sum_{i=1}^{N_r} p_i \delta(t - \tau_i), \tag{5}$$

Table 1. VLC Simulation Parameters [16,18,19]

Link Parameter	Value
Size of room	$5 \times 5 \times 3$ m^3
Number of lightings of commercial Cree LED	4
Number of chips per each lighting	100
Number of transmitted rays per chip	500,000
Transmitter viewing angle	120°
Area of rectangular PD	1 cm^2
Materials	Purely diffuse material
FOV of PD	85°
Power of each chip	0.45 W
Lighting positions	(1.5,1.5,2.85), (1.5,3.5,2.85), (3.5,1.5,2.85), (3.5,3.5,2.85)
Human reflection coefficient	0.1
Number of reflections for objects	7

where p_i and τ_i are the power and delay for the ith ray, respectively, and N_r is the total number of rays emitted by the LEDs. Accordingly, the channel DC gain H_0 is defined by Ref. [16]:

$$H_0 = \int_{-\infty}^{\infty} h(t)\mathrm{d}t. \tag{6}$$

The channel DC gain is considered one of the most important parameters needed in VLC channel modeling. The total received power at the receiver is defined by Ref. [14]:

$$P_r = P_t H_d(0) + \int P_t H_{\mathrm{ref}}(0), \tag{7}$$

where $H_d(0)$ and $H_d(0)$ are the DC channel gain of the direct and reflected paths, respectively, and P_t is the total optical transmitted power by LEDs. The better the channel gain, the better the received power. Accurate channel characterization is an important prerequisite to set the system parameters appropriately in order to establish a high-quality link, since it permits better exploitation of the available energy and spectral resources in view of optimizing the system design.

In Fig. 5, the histogram for the gain values that result from simulation is plotted, and several fitting distributions are also shown.

The degree of distribution fitting is evaluated using the log likelihood parameter, which indicates the degree of correlation of the distribution and channel gain data. The higher the log likelihood number, the better the accuracy of the distribution. The results obtained from the distribution fit toolbox in MATLAB reveal that the Nakagami channel for $m > 1$ shows a maximum log likelihood number of 1228.23, while log-normal distribution is placed second with a log likelihood number of 1226.45. The distribution fit toolbox in MATLAB [32] is used to represent the data using maximum likelihood estimation, and the resulted log likelihood parameter enables to identify the rank of the distributions that can fit the data. The greater the log likelihood number, the more distributions that can fit the data.

The results reveal that the Nakagami channel for $m > 1$ shows a maximum log likelihood number of 1228.23, while log-normal distribution is placed second with a log likelihood

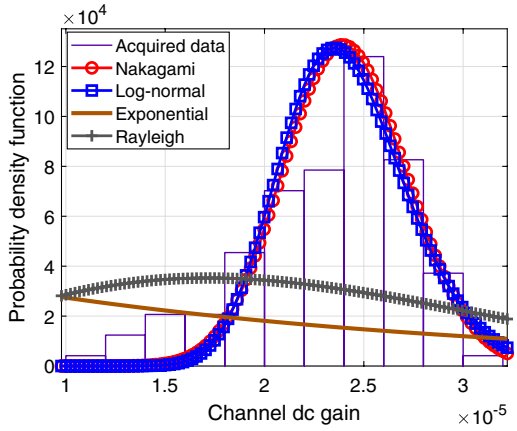

Fig. 5. Probability density function of the channel DC gain (H_0) of the VLC dynamic channel.

number of 1226.45. Both Rayleigh distribution and exponential distributions exhibit extremely poor fitting with log likelihood numbers of 1122.79 and 1049.92, respectively. Although Nakagami shows the best fitting with Zemax simulation results, we consider both Nakagami and log-normal distributions in our analysis because log-normal is commonly used with the analysis of RF systems [33,34]. The log-normal in our analysis can help authors that are interested in studying collaboration or comparison between RF and VLC systems.

Moreover, we consider the Nakagami distribution in this subsection and relate its parameters to include the effect of user density, as given in Ref. [14]. The PDF of Nakagami distribution is defined by Ref. [35]:

$$p_m(h_m) = \left(\frac{m}{\Omega}\right)^m \frac{2}{\Gamma(m)} {h_m}^{2m-1} \exp\left(\frac{-m h_m^2}{\Omega}\right), \quad (8)$$

where $h_m \geq 0$ is the VLC channel gain,

$$\Omega = \overline{h_m^2} = \int_0^\infty h_m^2 \times p_m(h_m) \mathrm{d}h_m \quad (9)$$

is the mean of gain square, and $m = \frac{\Omega^2}{\overline{(h_m^2 - \Omega)^2}} \geq \frac{1}{2}$.

Applying a random variable transformation in (8), the PDF of the electrical SNR γ_m can be written as

$$p_m(\gamma_m) = \left(\frac{m}{\Omega}\right)^m \frac{1}{\Gamma(m)} \left(\frac{1}{\xi\sqrt{\hat{\gamma}}}\right)^{2m} \left(\sqrt{\gamma_m}\right)^{2m-2} \times \exp\left(\frac{-m\gamma_m}{\Omega\hat{\gamma}\xi^2}\right), \quad (10)$$

where the instantaneous electrical SNR is related to channel instantaneous gain as follows [23]:

$$\gamma_m = \hat{\gamma}\xi^2 h_m^2 = \left(\frac{\mathcal{R}p_t}{\sigma_n}\right)^2 \xi^2 h_m^2. \quad (11)$$

Here, σ_n^2 is the variance of Gaussian noise, $\hat{\gamma}$ is the average optical SNR, and ξ is the modulation gain.

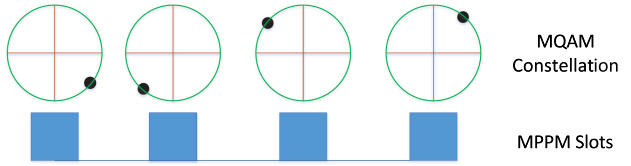

Fig. 6. Constellation of symbols in a hybrid MQAM–MPPM scheme.

The distribution parameters are the output of the distribution fit toolbox in our specific dynamic scenarios for Nakagami channel and are $m = 15.3$ and $\Omega = 5.914 \times 10^{-10}$, where the values of m and Ω depend on user speed and people density/meter in the room. Increasing m indicates worse channel conditions for the distribution expected to appear in this dynamic scenario due to severe multipath and shadowing fading. In Section 6, we consider different channel parameters for numerical analysis to indicate several channel scenarios, in order to validate the performance of hybrid and adaptive hybrid schemes at different channel conditions.

The study of dynamic VLC systems can be described by the log-normal distribution as it fits our DC gain data of the dynamic channel. The PDF of log-normal distribution is given by Ref. [36]:

$$p_l(h_l) = \frac{8.7}{h_l\sqrt{\left(2\pi\sigma_{h_l}^2\right)}} \exp\left(-\frac{\left(20\log_{10} h_l - \mu_{h_l}\right)^2}{2\sigma_{h_l}^2}\right), \quad (12)$$

where $h_l \geq 0$ is the instantaneous VLC channel gain, $\mu_{h_l} = 20\log_{10}\overline{h_l}$ is the mean of h_l in dB, $\overline{h_l}$ is the mean of h_l, and $\sigma_{h_l}^2 = \overline{(20\log_{10} h_l - \mu_{h_l})^2}$ is the variance of h_l in dB.

By applying the transformation of random variables in (12), the results reveal that the PDF of the SNR in the case of the log-normal channel can be written as

$$p_l(\gamma_l) = \frac{4.35}{\gamma_l\sqrt{\left(2\pi\sigma_{\gamma_l}^2\right)}} \exp\left(-\frac{\left(10\log_{10}\gamma_l - \mu_{\gamma_l}\right)^2}{2\sigma_{\gamma_l}^2}\right), \quad (13)$$

where $\mu_{\gamma_l} = 10\log_{10}\overline{\gamma_l}$, and $\sigma_{\gamma_l}^2 = \overline{(10\log_{10}\gamma_l - \mu_{\gamma_l})^2}$ is the variance of γ_l in dB. Here, $\overline{\gamma_l}$ is the mean of γ_l in dB.

The distribution parameters resulted from our specific scenarios for the log-normal channel are given as $\mu_{\gamma_l} = -10.6407$ and $\sigma_{\gamma_l} = 0.1319$.

4. BER PERFORMANCE ANALYSIS

In the hybrid MQAM–MPPM technique, optical power is transmitted during w signal slots only, where $w \in \{1, 2, \ldots, N\}$. Each of the w signal slots is modulated by one symbol of available M_q symbols of MQAM, as shown in Fig. 6.

In this section, we derive mathematical expressions for the average BER of the proposed hybrid modulation scheme over Nakagami and log-normal channels. Generally, the performance of the hybrid MQAM–MPPM technique is upper bounded based on averaging the effect of the two ordinary

schemes MQAM and MPPM as follows [37]:

$$\mathrm{BER}_b(\gamma_x) \le \frac{\log_2\binom{N}{w} + \frac{2^{L-2} w \log_2 M_q}{2^L - 1}}{\log_2\binom{N}{w} + w\log_2 M_q}\mathrm{BER}_{\mathrm{MPPM}}(\gamma_x) + \frac{w\log_2 M_q}{\log_2\binom{N}{w} + w\log_2 M_q}\mathrm{BER}_{\mathrm{MQAM}}(\gamma_x), \quad (14)$$

where $L = \left\lfloor \log_2\binom{N}{w} \right\rfloor$ is the number of bits coded by MPPM symbol, and $\gamma_x \in \{\gamma_m, \gamma_l\}$ is the instantaneous value of the SNR. Here, $\mathrm{BER}_{\mathrm{MPPM}}$ and $\mathrm{BER}_{\mathrm{MQAM}}$ are the instantaneous BER of the ordinary MPPM and MQAM, respectively, and upper bounded as in Ref. [22]:

$$\mathrm{BER}_{\mathrm{MPPM}}(\gamma_x) \le \frac{\left(\binom{N}{w} - 1\right)2^{L-1}}{2(2^L - 1)}\mathrm{erfc}\left(\sqrt{\frac{N\log_2\binom{N}{w}\gamma_x}{4w^2}}\right)$$

and

$$\mathrm{BER}_{\mathrm{MQAM}}(\gamma_x) \le \begin{cases} \frac{2\left(\sqrt{M_q}-1\right)}{\sqrt{M_q}k}\mathrm{erfc}\left(\sqrt{\frac{3M^2\gamma_x}{4(M_q-1)}}\right); & k \text{ even}, \\ \frac{2}{k}\mathrm{erfc}\left(\sqrt{\frac{3M^2\gamma_x}{4(M_q-1)}}\right); & k \text{ odd}, \end{cases} \quad (15)$$

where $k = \log_2 M_q$, and M_q is the number of bits per MQAM symbol.

The two ordinary schemes are independent, so the average BER of the hybrid scheme is obtained by obtaining the average of the ordinary schemes then substituting into Eq. (14).

The average BER the ordinary scheme over the VLC fading channel is given as

$$\overline{\mathrm{BER}} = \int_0^\infty \mathrm{BER}(\gamma_x)\cdot p(\gamma_x)\,\mathrm{d}\gamma_x. \quad (16)$$

Substituting Eqs. (15) and (10) into Eq. (16) and carrying out the integration [38], the BER of both of ordinary techniques for the Nakagami fading channel can be obtained as

$$\overline{\mathrm{BER}_{\mathrm{MPPM}}}(\hat{\gamma}) \le \frac{1}{\sqrt{\pi}\Gamma(m)}\left(\frac{m}{\Omega}\right)^m \frac{2^{L-1}\left[\binom{N}{w} - 1\right]}{2^{L+1} - 2} \times \left(\frac{1}{\xi\sqrt{\hat{\gamma}}}\right)^{2m}\left(\frac{L}{4N}\right)^{-m} G_{2,2}^{1,2}\left(\frac{4N\Omega}{m\xi^2\hat{\gamma}L}\Big|_{0,-m}^{1-m,0.5-m}\right), \quad (17)$$

where $G_{p,q}^{a,b}(\cdot|\cdot)$ is the Meijer G function, defined in Ref. [38].

Similarly, the average BER performance of the MQAM scheme over the Nakagami channel can be obtained as

$$\overline{\mathrm{BER}_{\mathrm{MQAM}}}(\hat{\gamma}) \le \begin{cases} \frac{\sqrt{M_q}-1}{\sqrt{\pi M_q}\Gamma(m)}\cdot\frac{2\left(\frac{m}{\Omega}\right)^m}{k}\left(\frac{1}{\xi\sqrt{\hat{\gamma}}}\right)^{2m}\left(\frac{3M^2}{4(M_q-1)}\right)^{-m} \times G_{2,2}^{1,2}\left(\frac{4(M_q-1)\Omega}{m\xi^2\hat{\gamma}3M^2}\Big|_{0,-m}^{1-m,0.5-m}\right); & k \text{ even}, \\ \frac{1}{\sqrt{\pi}\Gamma(m)}\frac{2\left(\frac{m}{\Omega}\right)^m}{k}\left(\frac{1}{\xi\sqrt{\hat{\gamma}}}\right)^{2m}\left(\frac{3M^2}{4(M_q-1)}\right)^{-m} \times G_{2,2}^{1,2}\left(\frac{4(M_q-1)\Omega}{m\xi^2\hat{\gamma}3M^2}\Big|_{0,-m}^{1-m,0.5-m}\right); & k \text{ odd}. \end{cases} \quad (18)$$

The overall BER of the hybrid scheme using the Nakagami channel is obtained by substituting Eqs. (17) and (18) into Eq. (14):

$$\mathrm{BER}_b(\gamma_m) \le \frac{\log_2\binom{N}{w} + \frac{2^{L-2} w \log_2 M_q}{2^L - 1}}{\log_2\binom{N}{w} + w\log_2 M_q}\frac{1}{\sqrt{\pi}\Gamma(m)}\left(\frac{m}{\Omega}\right)^m \frac{2^{L-1}\left[\binom{N}{w} - 1\right]}{2^{L+1} - 2}\left(\frac{1}{\xi\sqrt{\hat{\gamma}}}\right)^{2m}\left(\frac{L}{4N}\right)^{-m} \times G_{2,2}^{1,2}\left(\frac{4N\Omega}{m\xi^2\hat{\gamma}L}\Big|_{0,-m}^{1-m,0.5-m}\right) + \frac{w\log_2 M_q}{\log_2\binom{N}{w} + w\log_2 M_q} \begin{cases} \frac{\sqrt{M_q}-1}{\sqrt{\pi M_q}\Gamma(m)}\cdot\frac{2\left(\frac{m}{\Omega}\right)^m}{k}\left(\frac{1}{\xi\sqrt{\hat{\gamma}}}\right)^{2m}\left(\frac{3M^2}{4(M_q-1)}\right)^{-m} \times G_{2,2}^{1,2}\left(\frac{4(M_q-1)\Omega}{m\xi^2\hat{\gamma}3M^2}\Big|_{0,-m}^{1-m,0.5-m}\right); & k \text{ even}, \\ \frac{1}{\sqrt{\pi}\Gamma(m)}\frac{2\left(\frac{m}{\Omega}\right)^m}{k}\left(\frac{1}{\xi\sqrt{\hat{\gamma}}}\right)^{2m}\left(\frac{3M^2}{4(M_q-1)}\right)^{-m} \times G_{2,2}^{1,2}\left(\frac{4(M_q-1)\Omega}{m\xi^2\hat{\gamma}3M^2}\Big|_{0,-m}^{1-m,0.5-m}\right); & k \text{ odd}. \end{cases} \quad (19)$$

The BER of ordinary schemes under log-nomral fading channels can be obtained by substituting Eqs. (15) and (13) into Eq. (16) to get

$$\overline{\mathrm{BER}_{\mathrm{MPPM}}}(\mu_{\gamma_l}) \le \frac{\frac{2^L}{\sqrt{\pi}}\left[\binom{N}{w} - 1\right]}{2^{L+1} - 2}\sum_{i=1}^{n}\varphi_i \cdot Q\left(\sqrt{\frac{L10^{(X_i\sqrt{2}\sigma_{\gamma_l} + \mu_{\gamma_l})/10}}{2N}}\right), \quad (20)$$

and

$$\overline{\mathrm{BER}_{\mathrm{MQAM}}}(\mu_{\gamma_l}) \leq$$

$$\begin{cases} \frac{\sqrt{M_q}-1}{\sqrt{M_q}\frac{k}{4}} \sum_{i=1}^{n} \varphi_i Q\left(\sqrt{\frac{1.510^{\left(X_i\sqrt{2}\sigma_{\gamma_l}+\mu_{\gamma_l}\right)/10}}{M^{-2}(M_q-1)}}\right); & k \text{ even}, \\ \frac{4}{k} \sum_{i=1}^{n} \varphi_i Q\left(\sqrt{\frac{3M^2 10^{\left(X_i\sqrt{2}\sigma_{\gamma_l}+\mu_{\gamma_l}\right)/10}}{2(M_q-1)}}\right); & k \text{ odd}, \end{cases} \tag{21}$$

where X_i and φ_i are the i_{th} root and weight factors of the n_{th}-order Hermite polynomial for $i = \{1, 2, \ldots, n\}$, respectively [36].

The overall BER of the hybrid scheme using log-normal distribution can be obtained by substituting Eqs. (20) and (21) into Eq. (14):

$$\mathrm{BER}_h(\gamma_l) \leq \frac{\log_2\binom{N}{w} + \frac{2^{L-2} w \log_2 M_q}{2^L-1}}{\log_2\binom{N}{w} + w\log_2 M_q} \frac{\frac{2^L}{\sqrt{\pi}}\left[\binom{N}{w}-1\right]}{2^{L+1}-2} \sum_{i=1}^{n} \varphi_i \cdot Q\left(\sqrt{\frac{L10^{\left(X_i\sqrt{2}\sigma_{\gamma_l}+\mu_{\gamma_l}\right)/10}}{2N}}\right)$$

$$+ \frac{w\log_2 M_q}{\log_2\binom{N}{w} + w\log_2 M_q} \begin{cases} \frac{\sqrt{M_q}-1}{\sqrt{M_q}\frac{k}{4}} \sum_{i=1}^{n} \varphi_i Q\left(\sqrt{\frac{1.510^{\left(X_i\sqrt{2}\sigma_{\gamma_l}+\mu_{\gamma_l}\right)/10}}{M^{-2}(M_q-1)}}\right); & k \text{ even}, \\ \frac{4}{k} \sum_{i=1}^{n} \varphi_i Q\left(\sqrt{\frac{3M^2 10^{\left(X_i\sqrt{2}\sigma_{\gamma_l}+\mu_{\gamma_l}\right)/10}}{2(M_q-1)}}\right); & k \text{ odd}, \end{cases} \tag{22}$$

5. ADAPTIVE HYBRID MQAM–MPPM PERFORMANCE

The idea behind adaptive modulation techniques is to adapt the spectral efficiency based on channel status in order to avoid system outage and increase average spectral efficiency over time-varying channels. Moreover, the proposed adaptive process aims to transmit the top priority data rate at low data rates under worse channel conditions, while maintaining the maximum data rate at stable channel conditions. The proposed hybrid MQAM–MPPM technique has two degrees of freedom to change transmission spectral efficiency by changing settings of both MPPM and MQAM independently. This makes the hybrid scheme able to make gradual changes in spectral efficiency compared to the step changes in the ordinary MQAM technique. The adaptation process proceeds as follows: the transmitter and receiver measure the channel status through a sequence of training bits or any other advanced estimation scheme. Based on the channel status, both transmitters and receivers choose the modulation settings $\{N, w, M_q\}$ to keep the system BER performance at a specific level $\gamma \geq \gamma_{\mathrm{th}}$ and $\mathrm{BER} \leq \mathrm{BER}_{\mathrm{th}}$. The spectral efficiencies for MPPM, MQAM, and the hybrid schemes are given by Ref. [22]:

$$\eta = \begin{cases} \eta_m = \frac{\log_2\binom{N}{w}}{N}; & \text{for MPPM scheme}, \\ \eta_q = \log_2 M_q; & \text{for MQAM scheme}, \\ \eta_h = \frac{\log_2\binom{N}{w} + w\log_2 M_q}{N}; & \text{for hybrid scheme}. \end{cases} \tag{23}$$

A. Optimization Problem of Adaptive Constellation Scheme

In the adaptive hybrid modulation scheme, the constellation setting $\{N, w, M_q\}$ is adapted according to channel conditions. These parameters are key to hybrid adaptive modulation techniques, where $N \in \{2, 3, \ldots, N_{\max}\}$, $w \in \{1, 2, \ldots, N\}$, and $M_q \in \{4, 8, \ldots, M_{q_{\max}}\}$.

The total number of available settings $J_{\max}$ is

$$J_{\max} = \frac{\log_2\left(M_{q_{\max}}\right) N_{\max}\left(N_{\max}+1\right)}{2}. \tag{24}$$

Each $j \in \{1, 2, \ldots, J_{\max}\}$ setting has a specific spectral efficiency, given by Eq. (23), which helps in improving the SNR as in Eq. (11). The proposed adaptive scheme works for optimizing the average spectral efficiency, under the constraint of a given BER threshold ($\mathrm{BER}_{\mathrm{th}}$) and a range of received electrical SNR as

$$\gamma_{\max_j} > \gamma(h) \geq \gamma_{\min_j}, \quad j \in \{1, 2, \ldots, J_{\max}\}, \tag{25}$$

where $\gamma_{\min_j}$ indicates the minimum SNR at which the setting j achieves the BER threshold constraint ($\mathrm{BER}_{\mathrm{th}}$), which can be determined from Eqs. (14) and (15) for both hybrid and classic techniques, respectively. Here, $\gamma_{\max_j} = \gamma_{\min_{j+1}}$ and $\gamma_{\min_{J_{\max}+1}} = +\infty$.

We choose setting j, which achieves the highest spectral efficiency in the range of SNR. The optimization problem is well formulated as follows:

$$\begin{aligned} &\arg\max_{j\in\{1,2,\ldots,J_{\max}\}} \{\eta_{h_j}\} \\ &\text{Subject to :} \\ &\quad N \in \{1, 2, \ldots, N_{\mathrm{Max}}\},\ w \in \{1, 2, \ldots, N\}, \\ &\quad M_q \in \{1, 2, \ldots, M_{q_{\max}}\}, \\ &\quad \gamma_{\max_j} > \gamma(h) \geq \gamma_{\min_j}, \\ &\quad \mathrm{BER}_j \leq \mathrm{BER}_{\mathrm{th}}, \\ &\quad \{p_t, BW, \sigma_n\} \in \{\text{constant}\}, \end{aligned} \tag{26}$$

where BW is the bandwidth of the VLC channel, about 5–10 MHz for white LEDs.

The optimization in Eq. (26) is a discrete constrained optimization problem. Clearly, as the value of $J_{\max}$ becomes larger, the VLC transceivers become flexible to adapt their constellations and increase the channel throughput. However, increasing $J_{\max}$ would raise the physical complexity of the system as determined from (24).

B. Average Throughput

The average throughput (bit rate) of the total $J_{\max}$ constellation forms can be calculated by

$$\bar{R}_b = BW \sum_{j=1}^{J_{\max}} \eta_{b_j} \cdot \Pr\left(\gamma_{\max_j} > \gamma \geq \gamma_{\min_j}\right). \quad (27)$$

The probability of selecting jth setting is calculated from

$$\Pr\left(\gamma_{\max_j} > \gamma \geq \gamma_{\min_j}\right) = \int_{\gamma_{\min_j}}^{\gamma_{\max_j}} p(\gamma) d\gamma. \quad (28)$$

1. Nakagami Distribution

As for the Nakagami channel, the probability of selecting Jth setting is obtained as substituting (10) into (28). Using integration tables in Ref. [38], the probability is obtained as

$$\Pr\left(\gamma_{\max_j} > \gamma \geq \gamma_{\min_j}\right) = \left(\frac{m}{\Omega}\right)^m \frac{1}{\Gamma(m)} \left(\frac{1}{\xi_j \sqrt{\hat{\gamma}}}\right)^{2m} \times \left[-\gamma^m \left(\frac{m\gamma}{\Omega\hat{\gamma}\xi_j^2}\right)^{-m} \Gamma\left(m, \frac{m\gamma}{\Omega\hat{\gamma}\xi_j^2}\right)\right]\Big|_{\gamma_{\min_j}}^{\gamma_{\max_j}}. \quad (29)$$

2. Log-Normal Distribution

As for log-normal distribution, the probability of selecting j_{th} setting is given by substituting (13) into (28). Using the integration table of log-normal distribution, the probability is obtained as

$$\Pr\left(\gamma_{\max_j} > \gamma \geq \gamma_{\min_j}\right) = \times \frac{1}{2}\left[1 - \operatorname{erfc}\left(\frac{\gamma - \mu_{\gamma_l}}{\sqrt{2}\sigma_{\gamma_l}}\right)\right]\Big|_{10\log_{10}\gamma_{\min_j}}^{10\log_{10}\gamma_{\max_j}}. \quad (30)$$

We choose the minimum threshold according to certain criteria. If the actual SNR is below this threshold, outage will occur. So, we adjust the threshold to be the minimum of all configured settings.

C. Outage Probability

The outage probability for the system can be obtained from

$$p_{\text{out}} = \Pr(\gamma < \gamma_{\text{th}}) = \int_0^{\gamma_{\text{th}}} p(\gamma) \mathrm{d}\gamma, \quad (31)$$

where the value of SNR threshold γ_{th} can be obtained by

$$\gamma_{\text{th}} = \min_{j \in \{1,2,\ldots,J_{\max}\}} \left\{\gamma_{\min_j}\right\}. \quad (32)$$

Clearly, γ_{th} is joined with BER_{th}, where each BER threshold value has its corresponding SNR threshold value. At a given BER threshold, the corresponding SNR threshold can be obtained directly from (15), and for classic schemes, it can be obtained directly from (17) to (21). For the hybrid scheme, it can be obtained from (15) of the classic schemes and then substituting into the following equation [37]:

$$p_{\text{out}}^{\text{hybrid}} \leq 1 - \left(1 - p_{\text{out}}^{\text{MPPM}}\right)\left(1 - p_{\text{out}}^{\text{MQAM}}\right), \quad (33)$$

where $p_{\text{out}}^{\text{MPPM}}$ and $p_{\text{out}}^{\text{MQAM}}$ are the outage probabilities of classic MPPM and MQAM, respectively. Clearly, from (31) to (33), the system can reduce the signal quality in order to avoid link outage.

6. NUMERICAL RESULTS

In this section, we illustrate numerically the performances of hybrid schemes and compare them to those of ordinary schemes over both Nakagami and log-normal distributions. As mentioned in Section 5, we apply an optimization algorithm for the adaptation process. Consequentially, we are able to compare the adaptive hybrid schemes' performances with those of adaptive ordinary schemes from a spectral efficiency perspective in time-varying channels. Our simulation parameters are listed in Table 2, where the BER threshold is set to 10^{-3}, and the LED bandwidth is 10 MHz.

Furthermore, the maximum settings for MQAM and MPPM are restricted to $M_q \leq 16$ and $N \leq 60$, respectively. Also, the channel parameters (m, σ_{γ_l}) are selected to be in practical ranges [14] in order to validate the new adaptive hybrid technique under various channel conditions.

First, in Fig. 7, we compare the spectral efficiency of the adaptive hybrid scheme to that of both adaptive ordinary schemes over the time-varying Nakagami channel. We draw this figure by running an MC simulation, where the channel gain is generated based on a Nakagami distribution. Moreover, the optimization problem is solved for both hybrid and ordinary schemes to get the optimum modulation settings for all of them under generated channel gain.

As shown in Fig. 7, the spectral efficiency of the adaptive hybrid scheme outperforms that of both adaptive MQAM and MPPM classical schemes. Specifically, at low transmitted optical power of ≤ -30 dBm, the adaptive hybrid scheme achieves about three times higher bit rate than that of both MQAM and MPPM schemes. However, the increase in transmitted optical power leads to a reduced difference between achieved speeds of adaptive hybrid and adaptive MQAM schemes. This is because at high power, the hybrid scheme sends more data over the MQAM symbol by increasing both modulation level of used MQAM symbols and increasing the number of signal

Table 2. VLC Simulation Parameters [14]

Link Parameter	Value
Responsivity ($\mathcal{R}$)	0.5 A/W
Noise spectral density (N_o)	10^{-21}
Modulation index (M)	1
Bit-error rate threshold (BER_{th})	10^{-3}
Modulation bandwidth (BW)	10 MHz
MQAM ($M_{q,\max}$)	16
MPPM ($N_{\max}$)	60
Nakagami channel parameter (m)	{1,2,3}
Log-normal channel standard deviation (σ_{γ_l})	{3,4} dB

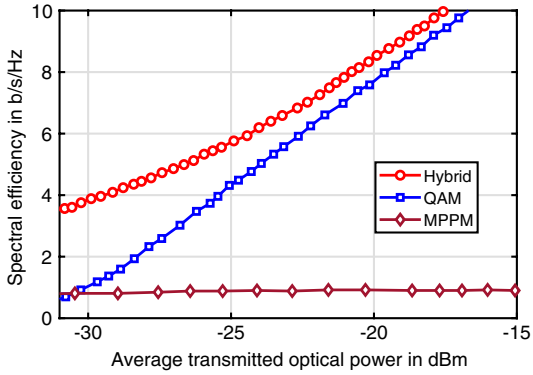

Fig. 7. Spectral efficiencies of adaptive hybrid scheme and both MQAM and MPPM adaptive ordinary schemes over Nakagami fading channel.

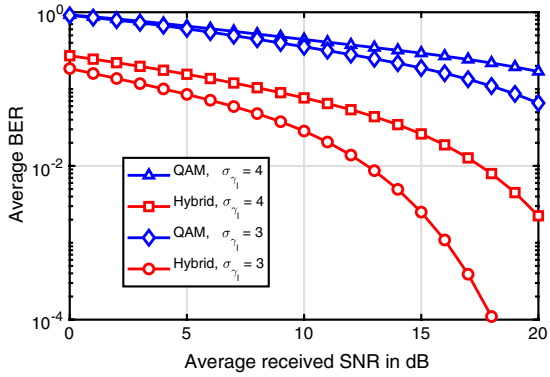

Fig. 8. Average BER of both hybrid ($N=4$, $w=2$, $M=1$, $M_q=8$) and MQAM ($M=1$, $M_q=4$) scheme over a log-normal channel.

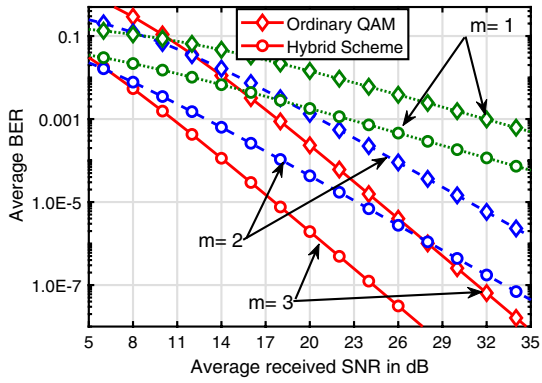

Fig. 9. Average BER of both hybrid ($N=4$, $w=2$, $M=1$, $M_q=8$) and MQAM ($M=1$, $M_q=4$) schemes over a Nakagami channel.

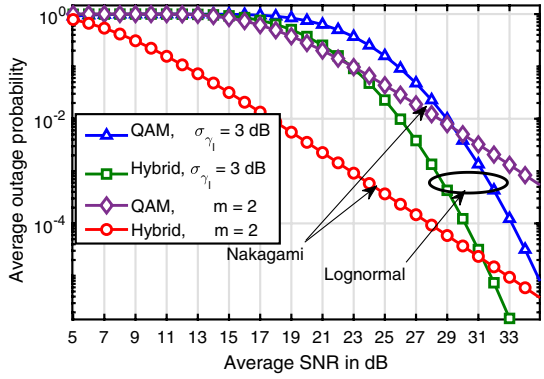

Fig. 10. Average outage probabilities for both hybrid ($M=1$, $M_q=8$, $N=4$, $w=2$) and MQAM ($M=1$, $M_q=4$) schemes over both Nakagami and log-normal channels at $\text{BER}_{\text{th}}=10^{-3}$.

slots reflected on increasing the number of MQAM symbols. When the optical power increases above a specific high value, the hybrid scheme will switch to sending signals all the time, which means it is converted to an ordinary MQAM mode.

Now, the BER and outage probability of both hybrid schemes and ordinary MQAM are compared under conditions of comparable spectral efficiencies, same bandwidth, and same energy per bit. The performance of ordinary MPPM is not considered in our comparison because its spectral efficiency is not comparable with both ordinary MQAM and the hybrid scheme.

In Fig. 8, the BERs of both hybrid and ordinary MQAM modulation schemes are plotted using log-normal distributions for two channel conditions ($\sigma_{\gamma_l} \in \{3, 4\}$ dB). Increasing the value of σ_{γ_l} indicates that the channel becomes worse, and this leads to worse BER performance for both schemes. In practice, changing channel conditions may indicate different people density or people movement. Generally, BER performance of the hybrid scheme with setting $\{N=4, w=2, M_q=8\}$ outperforms that of the ordinary MQAM scheme with setting $\{M_q=4\}$.

As shown in Fig. 9, the BER performance of the above modulation schemes under the Nakagami fading channel for three channel conditions is $m=\{1, 2, 3\}$.

Clearly, decreasing m indicates worse channel conditions, which leads to worse BER performance for all modulation schemes. In Fig. 9, it is noted that the hybrid scheme outperforms ordinary MQAM under the same channel state, and the difference in performance between them decreases as channel state improves. As shown in Fig. 9, the hybrid scheme shows 28%, 34%, and 38% improvement, respectively, for $m=1, 2, 3$ for Nakagami channels at $\text{BER}=10^{-3}$.

Figure 10 illustrates the performance of outage probability for hybrid $\{N=4, w=2, M_q=8\}$ and ordinary MQAM $\{M_q=4\}$ schemes over dynamic channels.

Moreover, Fig. 10 shows the outage probability of hybrid schemes of $\text{BER}=10^{-3}$, exhibiting 30% and 14% better performance than ordinary schemes is obtained. As shown in Figs. 8–10, clearly Nakagami has better performance than the log-normal channel, as it provides the best fitting for the dynamic channel gain obtained from previous results.

7. CONCLUSION

The performance of the adaptive hybrid MQAM–MPPM modulation technique under dynamic VLC channels has been investigated. The dynamic VLC channel is modeled by Nakagami and log-normal distributions based on the results of simulation using the Zemax solver. Each mobile user is carrying

a rectangular detector of fixed orientation. In our simulation, we have considered the effects of random people motions and practical human CADs, as well as the effects of coating materials for walls, ceiling, and floor. Expressions for average BER and outage probability of the hybrid scheme over VLC fading channels have been derived and compared numerically to that of ordinary schemes. Our results show that the hybrid scheme outperforms the ordinary ones for different channel states. Specifically, the hybrid scheme outperforms the ordinary MQAM in terms of SNR, as it can achieve 10^{-3} BER with SNR ≤ 7 dB for Nakagami with $m = 1, 2, 3$. As for the log-normal channel with $\sigma_{\gamma_l} = 3, 4$, the hybrid scheme can achieve 10^{-3} BER at average SNR ≤ 20 dB, while for the same SNR for the ordinary MQAM, the achieved BER is on the order of 10^{-1}. In addition, at an outage probability of 10^{-2}, the hybrid scheme shows an improvement of ≥ 8 dB for the Nakagami channel with $m = 2$, as well as an improvement of 3 dB for the log-normal channel with $\sigma_{\gamma_l} = 3$. Moreover, the adaptive hybrid scheme achieves three times higher bit rate than that of both ordinary schemes in terms of spectral efficiency assuming a fixed average power for the hybrid and ordinary schemes. The performance of the indoor VLC system is investigated under the influence of users' terminal mobility, including the impact of the high order of reflections for walls and objects. The obtained PDF due to dynamic channel gain variations and the novel expressions for BER and outage probability enable system designers to quantify the effects of user mobility. This is beneficial in designing handover, channel assignment algorithms and high-speed communications using adaptive modulation techniques and increasing spectral efficiencies by using new modulation techniques.

Disclosures. The authors declare no conflicts of interest.

REFERENCES

1. D. Karunatilaka, F. Zafar, V. Kalavally, and R. Parthiban, "LED based indoor visible light communications: state of the art," IEEE Commun. Surveys Tuts. **17**, 1649–1678 (2015).
2. M. Kashef, M. Abdallah, K. Qaraqe, H. Haas, and M. Uysal, "Coordinated interference management for visible light communication systems," IEEE/OSA J. Opt. Commun. Netw. **7**, 1098–1108 (2015).
3. S. Wu, H. Wang, and C. H. Youn, "Visible light communications for 5G wireless networking systems: from fixed to mobile communications," IEEE Network **28**, 41–45 (2014).
4. C. T. Manimegalai, S. Gauni, N. Raghavan, and T. R. Rao, "Investigations on suitable modulation techniques for visible light communications," in *International Conference on Wireless Communications, Signal Processing and Networking (WiSPNET)* (2017), pp. 1818–1822.
5. E. Morsy, H. A. Fayed, A. A. El-Aziz, and M. H. Aly, "DBPSK and DQPSK crosstalk in single-span WDM systems using DRA," Appl. Opt. **56**, 5583–5589 (2017).
6. K. O. Akande, P. A. Haigh, and W. O. Popoola, "On the implementation of carrierless amplitude and phase modulation in visible light communication," IEEE Access **6**, 60532–60546 (2018).
7. A. H. Azhar, T. A. Tran, and D. O'Brien, "Demonstration of high-speed data transmission using mimo-ofdm visible light communications," in *IEEE Globecom Workshops* (2010), pp. 1052–1056.
8. X. Liu, S. Chandrasekhar, T. H. Wood, R. W. Tkach, P. J. Winzer, E. C. Burrows, and A. R. Chraplyvy, "M-ary pulse-position modulation and frequency-shift keying with additional polarization/phase modulation for high-sensitivity optical transmission," Opt. Express **19**, B868–B881 (2011).
9. E. Agrell and M. Karlsson, "Power-efficient modulation formats in coherent transmission systems," J. Lightwave Technol. **27**, 5115–5126 (2009).
10. M. Karlsson and E. Agrell, "Generalized pulse-position modulation for optical power-efficient communication," in *37th European Conference and Exhibition on Optical Communication* (2011), pp. 1–3.
11. X. Liu, T. H. Wood, R. W. Tkach, and S. Chandrasekhar, "Demonstration of record sensitivities in optically preamplified receivers by combining PDM-QPSK and M-Ary pulse-position modulation," J. Lightwave Technol. **30**, 406–413 (2012).
12. H. S. Khallaf and H. M. H. Shalaby, "Proposal of a hybrid QAM-MPPM technique for optical communications systems," in *16th International Conference on Transparent Optical Networks (ICTON)* (2014), pp. 1–4.
13. A. S. El-Wakeel, N. A. Mohammed, and M. H. Aly, "Free space optical communications system performance under atmospheric scattering and turbulence for 850 and 1550 nm operation," Appl. Opt. **55**, 7276–7286 (2016).
14. P. Chvojka, S. Zvanovec, P. A. Haigh, and Z. Ghassemlooy, "Channel characteristics of visible light communications within dynamic indoor environment," J. Lightwave Technol. **33**, 1719–1725 (2015).
15. E. Sarbazi, M. Uysal, M. Abdallah, and K. Qaraqe, "Indoor channel modelling and characterization for visible light communications," in *16th International Conference on Transparent Optical Networks (ICTON)* (2014), pp. 1–4.
16. F. Miramirkhani and M. Uysal, "Channel modeling and characterization for visible light communications," IEEE Photon. J. **7**, 1–16 (2015).
17. A. E.-R. A. El-Fikky, M. E. Eldin, H. A. Fayed, A. A. El-Aziz, H. M. H. Shalaby, and M. H. Aly, "NLoS underwater VLC system performance: static and dynamic channel modeling," Appl. Opt. **58**, 8272–8281 (2019).
18. M. H. Behlouli, P. Combeau, S. Sahuguède, A. Julien-Vergonjanne, C. Le Bas, and L. Aveneau, "Impact of physical and geometrical parameters on visible light communication links," in *Advances in Wireless and Optical Communications (RTUWO)* (2017), pp. 73–76.
19. C. Le Bas, S. Sahuguede, A. Julien-Vergonjanne, A. Behlouli, P. Combeau, and L. Aveneau, "Human body impact on mobile visible light communication link," in *10th International Symposium on Communication Systems, Networks and Digital Signal Processing (CSNDSP)* (2016), pp. 1–6.
20. F. Miramirkhani, O. Narmanlioglu, M. Uysal, and E. Panayirci, "A mobile channel model for VLC and application to adaptive system design," IEEE Commun. Lett. **21**, 1035–1038 (2017).
21. Y. S. Eroglu, Y. Yapici, and I. Guvenc, "Impact of random receiver orientation on visible light communications channel," IEEE Trans. Commun. **67**, 1313–1325 (2019).
22. H. S. Khallaf, H. M. H. Shalaby, J. M. Garrido-Balsells, and S. Sampei, "Performance analysis of a hybrid QAM-MPPM technique over turbulence-free and gamma-gamma free-space optical channels," IEEE/OSA J. Opt. Commun. Netw. **9**, 161–171 (2017).
23. A. Bekkali, C. B. Naila, K. Kazaura, K. Wakamori, and M. Matsumoto, "Transmission analysis of OFDM-based wireless services over turbulent radio-on-FSO links modeled by gamma-gamma distribution," IEEE Photon. J. **2**, 510–520 (2010).
24. M. K. Simon, "A simple evaluation of DPSK error probability performance in the presence of bit timing error," IEEE Trans. Commun. **42**, 263–267 (1994).
25. K. Kiasaleh and T. He, "On the performance of DQPSK communication systems impaired by timing error, mixer imbalance, and frequency nonselective slow Rayleigh fading," IEEE Trans. Veh. Technol. **46**, 642–652 (1997).
26. K. Sato, T. Ohtsuki, I. Sasase, and S. Mori, "Performance analysis of (m, 2) MPPM with imperfect slot synchronization," in *Proceedings of IEEE Pacific Rim Conference on Communications Computers and Signal Processing* (1993), Vol. **2**, pp. 765–768.
27. K. Sato, T. Ohtsuki, and I. Sasase, "Performance of coded multi-pulse PPM with imperfect slot synchronization in optical

direct-detection channel," in *Proceedings of ICC/SUPERCOMM'94–1994 International Conference on Communications* (1994), Vol. **1**, pp. 121–125.
28. "Zemax 18 release 1, radiant Zemax LLC," 2018, https://www.radiantzemax.com/zemax.
29. "Grab CAD models," 2018, https://grabcad.com.
30. "Zemax programming language," 2018, https://customers.zemax.com/os/resources/learn/knowledgebase/what-is-zpl.
31. "Cree LEDs," 2018, http://www.cree.com.
32. The Mathworks Inc., MATLAB and Statistics Toolbox Release 2019b (2009).
33. H. Haas, "Visible light communication," in *Optical Fiber Communications Conference and Exhibition (OFC)* (2015), pp. 1–72.
34. K. H. Park, Y. C. Ko, and M. S. Alouini, "On the power and offset allocation for rate adaptation of spatial multiplexing in optical wireless MIMO channels," IEEE Trans. Commun. **61**, 1535–1543 (2013).
35. M. Lei, P. Zhang, H. Haas, and E. Costa, "Performance analysis of an adaptive modulation system over Nakagami-m fading channels," in *Vehicular Technology Conference. IEEE 55th Vehicular Technology Conference. VTC Spring 2002 (Cat. No.02CH37367)* (2002), pp. 1527–1531.
36. M. K. Simon and M. S. Alouini, "Digital communications over fading channels (M.K. Simon and M.S. Alouini; 2005) book review," IEEE Trans. Inf. Theory **54**, 3369–3370 (2008).
37. H. S. Khallaf, A. S. Ghazy, H. M. H. Shalaby, and S. S. A. Obayya, "Performance analysis of visible light communication systems over fading channels," in *19th International Conference on Transparent Optical Networks (ICTON)* (2017), pp. 1–4.
38. "Wolfram function site," 2018, http://functions.wolfram.com.